Proc. Int. Conf. Neutron Optics (NOP2017)
JPS Conf. Proc. **22**, 011014 (2018)
https://doi.org/10.7566/JPSCP.22.011014

Study of Neutron Phase Diffraction Grating at Very High Resolution SANS Diffractometer KWS3

Alexander IOFFE and Vitaliy PIPICH

Jülich Centre for Neutron Science at Heinz Maier-Leibnitz Zentrum, Forschungszentrum Jülich GmbH, Garching, 85747 Germany

**E-mail: a.ioffe@fz-juelich.de*

(Received October 7, 2017)

The very high resolution focusing SANS diffractometer KWS3, providing the Q-resolution of about 3.8×10^{-5}Å^{-1} at λ=12.8Å, is used for studies of the phase diffraction grating with the rectangular surface relief (the period of 3.3μm) obtained by photolithography and electrolytic deposition of Ni. Multiple diffraction orders are simultaneously recorded using a high-resolution 2-D position-sensitive detector.

The presence of even diffraction orders in the angular spectrum is explained by non-rectangular trapezoidal-like distortions of the surface relief, which is reconstructed using the expansion in the Fourier series. The inclination of the grating leads to the increase in the phase modulation and, in turn, in higher intensity of high diffraction orders allowing for retrieving sharp features of the surface relief.

KEYWORDS: phase diffraction grating, very high resolution SANS

1. Introduction

Similar to well-known optical diffraction gratings, neutron diffraction gratings provide periodical modulation of the incident neutron wave, so that the scattered wave consists of several neutron beams propagating in different directions (diffraction orders). The modulation of the incident neutron wave may be achieved either by the modulation of its amplitude or phase: such gratings are called amplitude or phase gratings, respectively.

Neutron diffraction gratings have being used for the construction of neutron interferometers [1, 2] for purposes of fundamental physics [3, 4]. In the last decade neutron grating interferometry has become a standard tool for the neutron imaging [5].

Here we present the first results of the study of the Ni phase diffraction grating using the very high resolution focusing SANS diffractometer KWS3 of JCNS at MLZ, that provides a very high Q-resolution of about 3.8×10^{-5}Å^{-1} at λ=12.8Å and allows for the simultaneous recording multiple diffraction orders.

2. Neutron diffraction gratings

The phase diffraction grating used in this study has been prepared by the procedure similar to one described in [6]. First, a thin copper layer is deposited on a flat glass substrate and then spin-coated by a thin layer of positive photoresist (Fig 1). Second, the photoresist is exposed to UV light through a computer-drawn chromium mask

consisting of 1.65μm wide stripes separated by 1.65μm (both are noted as *d/2* in Fig. 1); then unexposed photoresist is dissolved away thus opening access to the copper stripes. Finally, the negative electrode is connected to the copper layer that acts as the cathode and a layer of nickel is electrolytically deposited onto the copper stripes through the windows in the photoresist mask, thus creating a binary Ni diffraction grating.

The deposition rate is defined by the current and is selected to be about 0.2μm/min. For such slow deposition rates, a high accuracy in the thickness *h0* of the deposited Ni is achieved by the control of the deposition time. This thickness *h0* defines the wavelength λ at which the phase difference between neutrons propagating through the Ni stripes and through the grooves between them is 180°:

$$h0 = \frac{\lambda}{2(n-1)} \tag{1}$$

where

$$n = 1 - \frac{\lambda^2 \rho_{Ni}}{2\pi} \tag{2}$$

is the neutron refraction index of Ni at wavelength λ (ρ_{Ni} - the scattering length density of Ni.) The grating we used in this study has been optimized for λ=20Å, that corresponds to h_0=1.74μm.

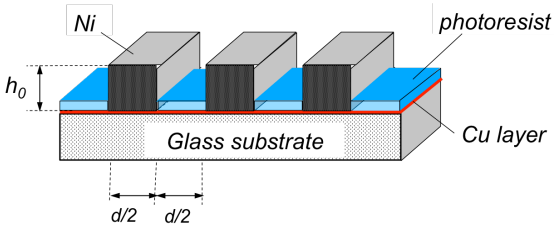

Fig. 1. Layout of the phase diffraction grating with period d = 3.3μm

3. Diffraction on the phase grating

Transmission through the 1-D phase diffraction grating with period *d* is described by the transmission function

$$T(x) = \sum_{n=-N}^{N} \exp\left[i\varphi(x - nd)\right] \tag{3}$$

where $\varphi(x)$ is the phase acquired after the propagation of the neutron wave through the single stripe.

The intensity distribution at the detector placed at a large distance from the grating (the condition of the Fraunhofer diffraction) is the Fourier transform $\{F[T(x)]\}^2$ and consists of *(2m+1)* discrete diffraction orders with intensities $I_m = I_{inc}\eta_m$, where I_{inc} is the incident beam intensity and η_m is the diffraction efficiency of the phase grating for the *m-th* order ($m \neq 0$)

$$\eta_m = \frac{4}{\pi^2 m^2} \tag{4}$$

The transmission function can be presented using the sum of harmonics

$$T_{meas}(x) = \sum_{m=1}^{M} \eta_m \cos\left(\frac{2\pi m}{d} x\right) \tag{5}$$

so that measuring the intensity of diffraction orders one can reconstruct *T(x)* and visualize the phase modulation provided by a single grating's stripe - the main quality parameter of the phase diffraction grating.

Such an approach was used in [7], where intensities of diffraction orders from diffraction gratings with periods 12μm and 20μm have been determined by the high-resolution double crystal diffractometer and the SESANS setup. As the result, the surface profile of the used phase diffraction gratings was restored with a high accuracy.

Another instrument that can be used for diffraction studies at such length scale is the very high resolution SANS diffractometer KWS3 providing a Q-resolution up to 3×10^{-5}Å^{-1} in the wavelength range (10-30)Å [8]. The principle of the operation of this diffractometer is based on the use of 2-D focusing of neutrons by a toroidal mirror, so that the entrance aperture (see Fig. 2) is imaged to the 2-D detector in the scale 1:1. If the diffraction grating is placed just after the focusing mirror as it is shown in Fig. 2, each of diffraction orders will create a separate image of the entrance aperture at the detector.

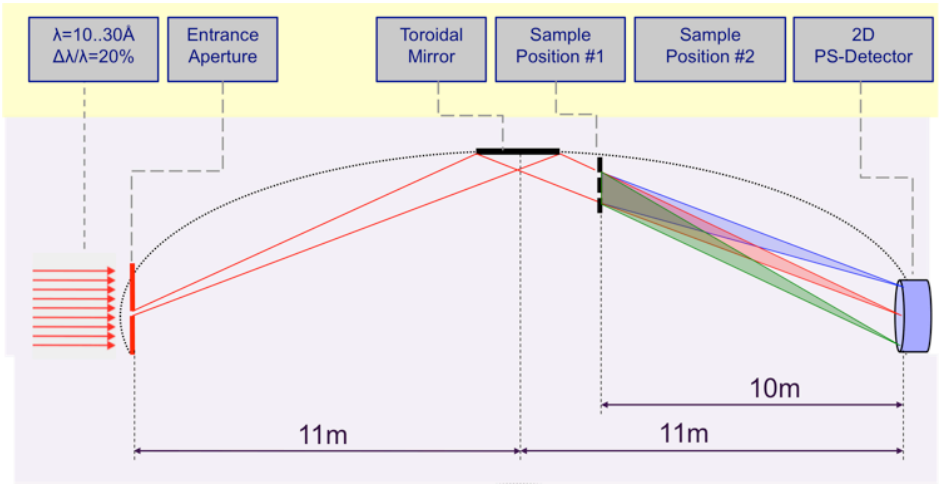

Fig. 2. Layout of the experiment at the SANS diffractometer KWS3. The phase diffraction grating is placed at the sample position 1.

4. Experiment

The phase grating described in the previous section was installed perpendicular to

the neutron beam just after the focusing mirror; the stripes of the grating were oriented vertically to avoid gravitational distortions of images. As in this case we are dealing with the one dimensional diffraction, the entrance aperture is set to a vertical slit with the size of $(0.4 \times 15)\text{mm}^2$. The recorded 2-D diffraction pattern is presented in Fig. 3. The black dots are 1-D intensity distributions obtained by integration over vertical direction (corrected to the transmission of glass substrate). The red dots represent the image of the entrance aperture that is broadened by the resolution function of the instrument centered around the momentum transfer Q_0:

$$R(Q) = \frac{1}{\sqrt{2\pi}\sigma} e^{-\frac{1}{2}\left(\frac{Q-Q_0}{\sigma}\right)^2} \tag{6}$$

where Q is the momentum transfer, and σ is the FWHM of the incident beam.

The symmetrical intensity distribution for the diffracted beam (black dots) clearly demonstrates the presence of three diffraction orders; widths of the peaks are again determined by the resolution function $R(Q)$ with $\sigma = 3.8\times10^{-5}$ Å^{-1}.

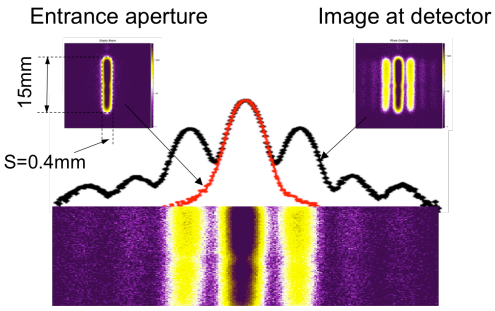

Fig. 3. 1-D diffraction pattern recorded by position sensitive detector.

Seven diffraction orders (m=0-6) are recorded in one measurement by the $(30 \times 30)\text{mm}^2$ high-resolution detector with a pixel size of about 110μm. To increase the Q-coverage more diffraction orders are recorded at three different (however slightly overlapping) detector positions in the horizontal plane; the combined diffraction pattern is presented in Fig. 4. Diffraction orders up to m=6 are clearly observed, while the observation of higher diffraction orders is handicapped by the effect of resolution (Fig. 5), which is very high at low Q where it is defined by the size of the entrance aperture and low at higher Q, where the spectral width of the incident neutron beam, $\Delta\lambda/\lambda$=15%, dominates [9].

For the ideal binary diffraction grating (see Fig.1), the Fourier coefficients can be calculated as

$$a_m = \frac{1}{d}\int_{-d/4}^{d/4} e^{-jk\frac{2\pi}{d}x}\,dx = \frac{1}{m\pi} Sin\left(m\frac{\pi}{2}\right)$$

Thus, a_m are equal to zero for all even m and even diffraction orders should be absent in the diffraction pattern.

However, the diffraction pattern presented in Figs. 3 and 4 shows the presence of such diffraction orders, which result from the sinusoidal-like, rather than binary, character of the phase modulation. Indeed, the diffraction grating is not perfect and

using eq. (5) with weights η_m equal to the experimentally determined diffraction efficiencies one can restore the function $T_{meas}(x)$ that is an approximation to the real surface profile. As the intensity of higher orders descends as $1/m^2$ (see eq. (4)), the accurate determination of the fine details of the profile requires accurate measurements and therefore rather long acquisition times.

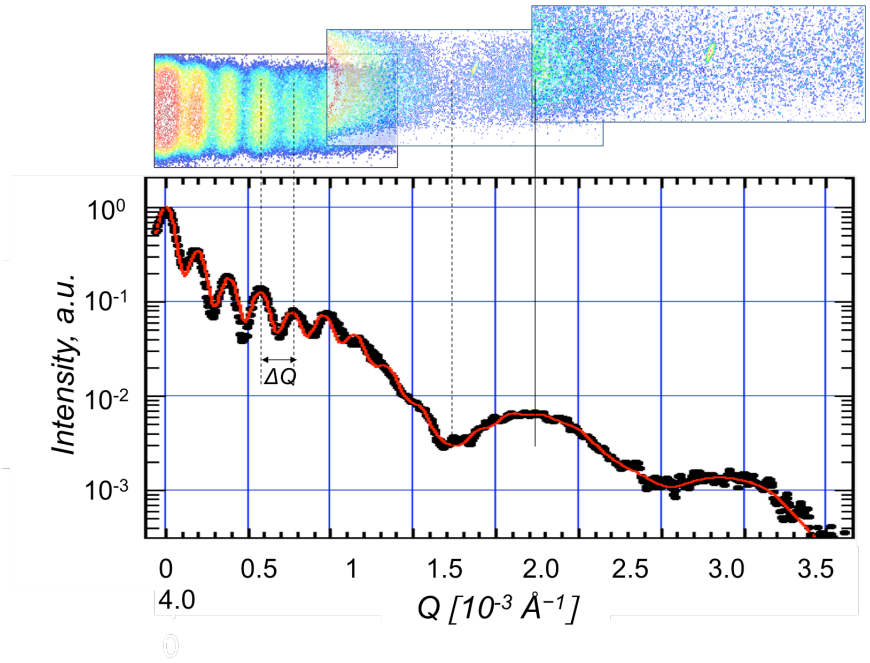

Fig. 4. Intensity distribution in the diffraction pattern. Black dots –row data (each dot corresponds to one detector pixel). Red curve is obtained the convolution of row data with the resolution function $R(Q)$ (σ=3.8·10^{-5}Å^{-1}). Background corrections are not applied.

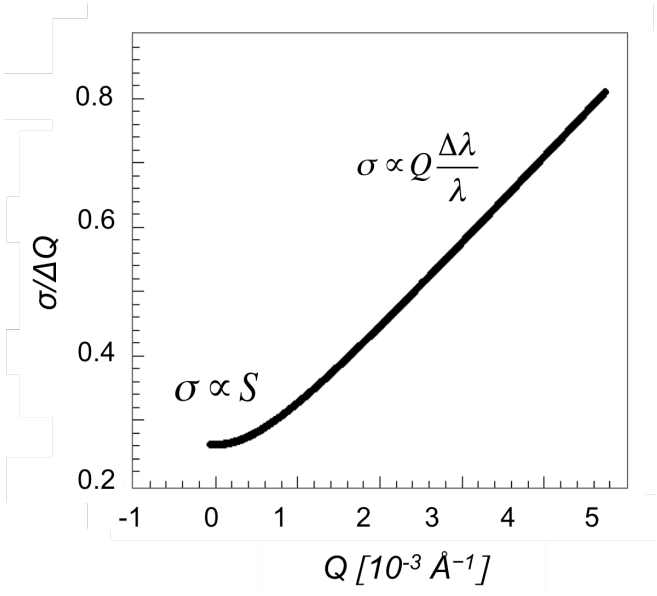

Fig. 5. Q-dependence of the resolution function of KWS3.

For the true sinusoidal phase grating the normalized intensity of the diffraction orders is described by the Bessel functions of order m:

$$\eta_m^{Ideal}(\varphi) = \frac{I_m}{I_{inc}} = \left[J_m(\varphi)\right]^2 \tag{7}$$

where φ is the magnitude of the phase modulation created by the phase grating (Fig. 6).

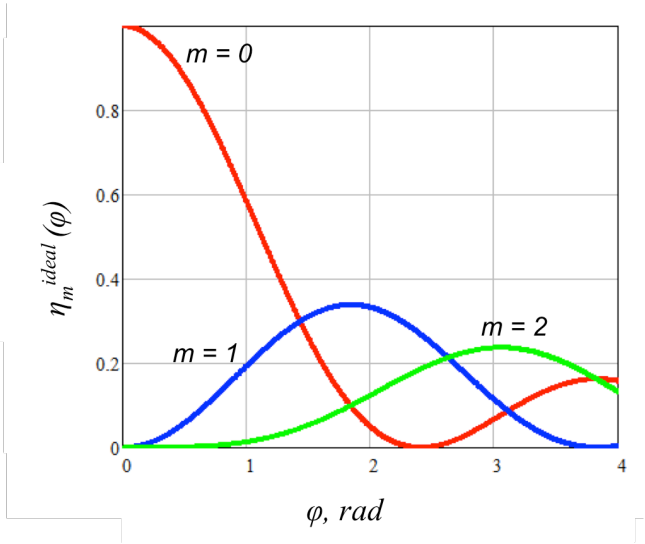

Fig. 6. Diffraction efficiencies of the sinusoidal phase grating.

In our case, φ is the phase acquired by neutron waves propagating through the Ni stripes and can be changed by the inclination of the grating (Fig. 7, left panel) that results in the increase of the optical path through the Ni stripe (red line), so that (Fig. 7, right panel)

$$\varphi(\alpha) = \frac{2\pi}{\lambda}(1-n)\cdot s = Nb\lambda\frac{h_0}{\sin(\alpha)} \tag{8}$$

where α is the angle of incidence on the grating.

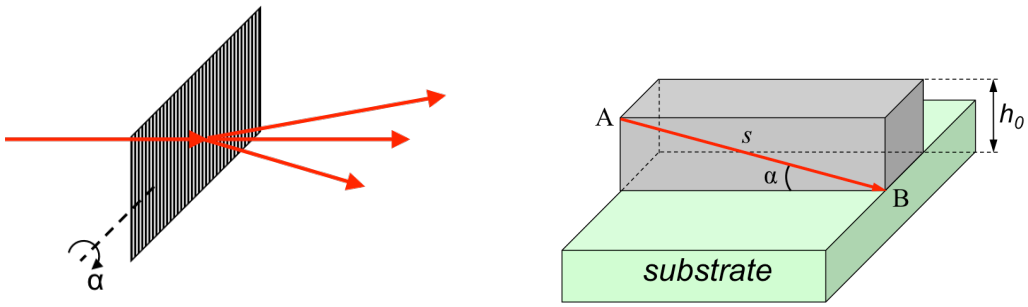

Fig. 7. Inclination of diffraction grating (left panel) results in the increase of the optical path shown by red line (right panel).

Intensity distributions in diffraction patterns were recorded for a number of incident angles in the range from 10° to 90°; distributions for angles 90°, 44°, 23° and 10° are shown in Fig. 8.

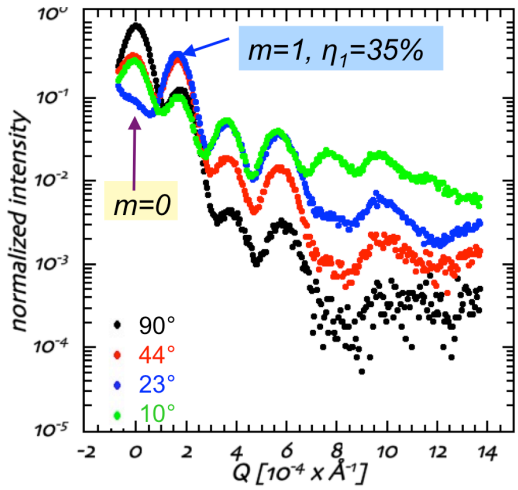

Fig. 8. Intensity distributions in the diffraction pattern for different inclination angles of the grating. Background corrections are applied.

We can compare the φ-dependences of measured diffraction orders with ones of sinusoidal phase grating shown in Fig. 6 (see also eq. (7)). For α=44° that corresponds to φ = 2.897 (red curve in Fig. 8) the magnitudes of m=0 and m=1 diffraction orders are equal. However, this is twice as much as one expects from the ideal grating, φ = 1.435 (see Fig. 6). For α=23° that corresponds to φ = 5.151 (blue curve in Fig. 8) the magnitude of m=1 diffraction order is maximal. This is also much higher than one expect from the ideal sinusoidal grating, where η_m^{Ideal} is maximal at φ = 1.84 (see Fig. 6).

From this one can conclude that the shape of the grating stripes is not rectangular, but also not sinusoidal; the stripe's shape is close to trapezoidal (as an intermediate between rectangular and sinusoidal). This is consistent with the electrolytic process used for the growing Ni bars: some Ni atoms may be deposited on the sides of the growing bar. Such broadening will be linearly decreased towards the top of the bar, because of the linear decrease of the time (from bottom to top) the bar is exposed to the electrolyte.

In order to obtain the function $T_{exp}(x)$ using Eq. (5), one should measure as many high diffraction orders as possible, because they contain the information about fine structure of the stripe's shape. Moreover, the weight of these orders should be large enough to make corresponding terms more significant. However, as one can see from Fig. 8, the contribution of higher orders at normal incidence on the grating (α =90°) is rather small, up to fractions of a percent.

As it was shown above, the diffraction efficiency of higher orders is significantly enhanced for the inclined grating, when the incident wave propagates longer distances in the Ni stripe and therefore accumulates a larger phase (see Fig. 7, right panel).

Reconstructed functions $T_{exp}(x)$ obtained using measured diffraction efficiencies coefficients η_m from measurements at different angles α (Fig. 8) are shown in Fig. 9.

One can see that accounting for higher diffraction orders (which are related to higher spatial frequencies) better measured at larger inclinations of the grating and allows for retrieving sharp features of the surface relief.

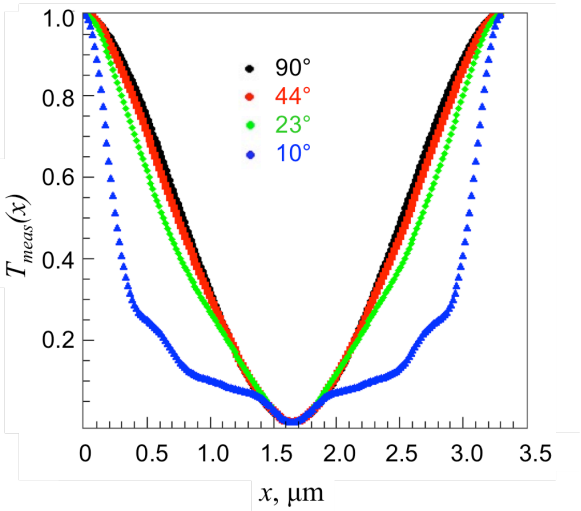

Fig. 9. Reconstructed functions $T_{exp}(x)$ obtained using measured diffraction efficiencies.

4. Conclusion

The very high resolution focusing SANS diffractometer KWS3 of JCNS at MLZ proved to be an effective instrument for studies of fine features of neutron diffraction gratings. Six diffraction orders have been recorded using a 2-D position-sensitive detector with very high spatial resolution, that allows for the Q-resolution of about $3.8 \cdot 10^{-5} Å^{-1}$ at λ=12.8Å.

The presence of even diffraction orders in the angular spectrum is explained by non-rectangular trapezoidal profile of the surface relief, which can be restored using the expansion in the Fourier series.

The inclination of the grating allows for a significant increase in the diffraction efficiency for higher diffraction orders carrying the information about higher spatial frequencies responsible for fine details of the phase profile.

References

[1] A.Ioffe, Yu.Turkevitch and G. Drabkin: JETP Letters 33, 374 (1981).
[2] M.Gruber, K.Eder, A.Zeilinger, R.Gähler and W.Mampe: Phys. Lett. A140, 363 (1989).
[3] A.Ioffe: Nucl. Instrum. Meth. A209, 343 (1984).
[4] J. Baumann, R. Gähler, A.Ioffe, J.Kalus and W.Mampe: Nucl. Instr. Meth. A284, 130 (1989).
[5] F. Pfeiffer: AIP Conference Proceedings 1466, 2 (2012).
[6] P. D. Kearney, A. G. Klein, G. I. Opat, and R. A. Gahler: Nature (London) 287, 313 (1980).
[7] M.Trinker, E.Jericha, W.G.Bouwman, R.Loidl and H.Rauch: Nucl. Instr. Meth. A579, 1081 (2007).
[8] V. Pipich and Zh. Fu, J. Large-scale Research Facilities, **A31**, 1 (2015).
[9] D.F.R. Mildner: J.Appl.Cryst. 38, 488 (2005).